Photoacoustic-MR Images Registration Based on Co-Sparse Analysis Model to Compensate for Brain Shift

Parastoo Farnia, Bahador Makkiabadi, Maysam Alimohamadi, Ebrahim Najafzadeh, Maryam Basij, Yan Yan, Alireza Ahmadian*, Member, *IEEE*, and Mohammad Mehrmohammadi*, Member, *IEEE*

***Abstract*— Brain shift is an important obstacle for the application of image guidance during neurosurgical interventions. There has been a growing interest in intra-operative imaging systems to update the image-guided surgery systems with real-time data. However, due to the innate limitations of the current imaging modalities, accurate and real-time brain shift compensation remains as a challenging problem. In this study, application of the intra-operative photoacoustic (PA) imaging and registration of the intra-operative PA images with pre-operative brain MR images is proposed to compensate brain deformation during surgery. Finding a satisfactory multimodal image registration method is a challenging problem due to complicated and unpredictable nature of brain deformation. In this study, the co-sparse analysis model is proposed for PA-MR image registration which can capture the interdependency of two modalities. The proposed algorithm works based on the minimization of mapping transform by using a pair of analysis operators. These operators are learned by the alternating direction method of multipliers. The method was evaluated using experimental phantom and ex-vivo data obtained from mouse brain. The results of phantom data show about 60% and 63% improvement in root mean square error (RMSE) and target registration error (TRE) in comparison with commonly used normalized mutual information registration method. In addition, the results of mouse brain and phantom data shown more accurate performance for PA versus ultrasound imaging for brain shift calculation. Finally, by using the proposed registration method, the intra-operative PA images could become a promising tool when the brain shift invalidated pre-operative MRI.**

***Index Terms*— Brain shift, Co-sparse analysis, Intra-operative imaging, Multimodal image registration, Photoacoustic imaging.**

Parastoo Farnia, Ebrahim Najafzadeh, and Alireza Ahmadian are with the Medical Physics and Biomedical Engineering Department, Faculty of Medicine, Tehran University of Medical Sciences (TUMS), Tehran, Iran, and with the Research Centre of Biomedical Technology and Robotics (RCBTR), Imam Khomeini Hospital Complex, Tehran University of Medical Sciences, Tehran, Iran. Bahador Makkiabadi is with the Medical Physics and Biomedical Engineering Department, Faculty of Medicine, Tehran University of Medical Sciences (TUMS), Tehran, Iran. Maysam Alimohamadi is with the Brain and spinal cord injury research center, Neuroscience Institute, Tehran University of Medical Sciences (TUMS), Tehran, Iran. Maryam Basij and Yan Yan are with the Department of Biomedical Engineering, Wayne State University, Detroit, Michigan, USA. Mohammad Mehrmohammadi is with the Department of Biomedical Engineering, Wayne State University, Detroit, Michigan, USA, and Barbara Ann Karmanos Cancer Institute, Detroit, Michigan, USA. (*Corresponding authors' email: mehr@wayne.edu, ahmadian@sina.tums.ac.ir.).

I. Introduction

Maximal Safe resection of brain tumors in eloquent regions is optimally performed under image-guided surgery systems [1, 2]. Accuracy of the image-guided neurosurgery system is drastically affected by intra-operative tissue deformation, called brain shift. Brain shift is a dynamic complex spatiotemporal phenomenon which happens after performing a craniotomy and invalidates pre-operative image of patients [3, 4]. Brain shift which is known as the brain deformation is a combination of the wide variety of biological, physical and surgical causes and occurs at both cortical and deep brain structures [2, 5-7]. Brain shift calculation and compensation methods are based on updating the pre-operative images with regard to the intraoperative tissue deformation. These methods fall into two main categories: biomechanical models and intra-operative imaging approaches. Biomechanical model-based approaches are time and computation consuming methods; however, they could be highly accurate [8-10]. The main challenge of model-based methods is that the tissue deformations occur during intraoperative neuro-surgical procedures are hard to accurately and real time model and thus are often not considered [2]. Therefore, most of the recent studies focused on using intra-operative imaging including intraoperative computed tomography (CT) [11], magnetic resonance imaging (MRI) [12-14], fluorescence-guided surgery [15], and ultrasound (US) imaging [16-18] during neurosurgery. In fact, interventional imaging systems are becoming an integral part of modern neurosurgeries to update patients coordinate during surgery using registration of intra-operative images with pre-operative images [19]. However, each of these modalities are proved to have well-known limitations [20]. Radiation exposure and low spatial resolution in CT, the requirement of an expensive equipped MR compatible operating room and time consuming for MRI, limited imaging depth in fluorescence imaging, and poor quality of the US images are the major challenges of the common intra-operative imaging modalities [21].

Recently, application of the hybrid imaging modalities such as photoacoustic (PA) imaging has gained considerable interest for various applications such as differential diagnostic of pathologies [22, 23], depicting tissue vasculature [24], oral health [25, 26] and image-guided surgeries [27-29]. The PA is a non-ionizing hybrid imaging method which combines optical and ultrasound imaging modalities based on the PA e□ect: the formation of sound waves following pulsed light absorption in a medium [30-32]. PA imaging inherits advantages of high imaging contrast from optical imaging as well as the spatial and temporal resolution of the US imaging [33-37]. During PA image acquisition, the tissue is illuminated by short laser pulses, which is absorbed by endogenous (or exogenous) chromophores, and cause the generation of ultrasound emission due to thermoelastic expansion. Endogenous chromophores such as hemoglobin provide a strong PA signal due to high optical absorption coe□cients which in turn demonstrates the crucial structural information [30, 38]. One of the main advantages of PA imaging is the ability to visualize the blood vessel meshwork of brain tissue which is considered as the main landmark during neurosurgery [21, 39, 40]. In the other hand, PA imaging has demonstrated potential to be used during image-guided interventions [41-43]. Therefore, PA imaging as a noninvasive intra-operative imaging could enable the real-time visualization of regions of interest including vessel meshwork during neurosurgery. Finally, registration of intra-operative PA images with pre-operative MR images of brain tissue could enables for real time compensation of brain shift.

Many investigations have tried to overcome the limitations of multimodal image registration algorithms in processes of brain shift compensation. Nevertheless, finding a single satisfactory solution is a challenging task due to the complex and unpredictable nature of the brain deformation during neurosurgery [44]. So far, most of the studies have focused on registration of intra-operative US with pre-operative MR algorithms. Major findings reported by Reinertsen et. al. [45], Chen et. al. [46], and Farnia et. al. [47] via feature-based registration methods. However, extraction of the corresponding features in two different modalities is an issue which directly affects the accuracy of these methods. In the intensity-based area, the different nature of US and MRI contrast mechanisms, leads to failure of the common similarity measures such as mutual information [48, 49]. However, effective solutions have been proposed by Wein et. al. [50], Coupé et. al. [51], Rivas et. al. [52, 53] and Machado et. al. [54] for multimodal image registration which face different limitations.

Recently, multimodal image registration based on sparse representation of images has attracted enormous interest. The main idea of image registration based on sparse representation lies on the fact that different images can be represented as a combination of a few atoms in an over-complete dictionary [55]. Therefore, the sparse coefficients describe the salient features of the images. Generally, over-complete dictionaries could be constructed via two different approaches. In the first category, standard fixed transform is applied as an over-complete dictionary. Fixed dictionaries such as discrete cosine transform, wavelet and curvelet are used for multi-modal image registration [19, 56, 57]. Using fixed dictionaries benefits from simplicity and fast implementation. However, it is not customized for different types of data. In the second approach, an over-complete dictionary was constructed via learning methods. Among learning methods, the K-singular value decomposition (K-SVD) method has been widely used for image registration [58]. There are some studies which used synthesis sparse models for multimodal image registration [59]. However, a learned dictionary includes a large number of atoms. This leads to increase computational complexity of multi-modal image registration which is not suitable for real time compensation of brain shift.

The analysis sparse model; named co-sparse analysis model, represents a powerful alternative to the synthesis sparse representation approach in order to reduce the computational time [60]. Co-sparse analysis models can yield richer feature representations and better results for image registration in real time processes [61, 62]. There are few studies for multi-modal image registration via co-sparse analysis model, and none of them were in the medical field. Kiechle et. al. proposed analysis model in a joint co-sparsity setup for different modalities of depth and intensity images [63]. Chang Han et. al utilized the analysis sparse model for remote sensing images [64] and Gao et. al. used it to register multi-focus noisy images with higher quality images [65]. In our previous work, we could apply an analysis sparse model for US-MR image registration to compensate the brain shift [66].

To date, a few research studies investigated PA and MR image registration. Ren et. al. proposed PA-MR image registration method based on mutual information to yield more insights into physiology and pathophysiology [67]. Gehrung et. al. proposed co-registration of PA and MR image of murine tumor models for assessment of tumor physiology [68]. However, these studies were dedicated to solve the rigid registration problems and also did not focus on intra-operative application of PA imaging, and therefore did not face any complicated brain deformation.

To the best of our knowledge, in this study for the first time, PA and MR images registration was used for the purpose of compensating complicated brain shift phenomena. The co-sparse analysis model is proposed for PA-MR image registration which is able to capture the interdependency of two modalities. The algorithm works based on the minimization of mapping transform by using a pair of analysis operators which are learned by the alternating direction method of multipliers (ADMM).

II. Materials and Methods

A. *Brain-mimicking phantom data*

To assess the performance of the multi-modal image registration algorithm to compensate brain shift, a phantom that mimics brain tissue was prepared. The phantom was made of Polyvinyl Alcohol Cryogel (PVA-C) which have been successfully used for mimicking brain tissue in previous studies [19, 47]. The PVA-C material also has been applied in the fabrication of phantoms for ultrasound, MRI and recently PA imaging [69]. A 10% by weight PVA in water solution was used to form PVA-C, which is solidified through a freeze–thaw process. The dimensions of the phantom were approximately 150 mm× 40 mm, with a curved top surface mimicking the shape of a head as shown in Fig. 1 (a). Two plastic tubes with 1.2 and 1.4 mm inside diameters were inserted randomly to the mold before freeze–thaw cycle to simulate blood vessels. Fig. 1. b shows the 3D model of the phantom including random vessels. Two types of chromophores; copper sulfate pentahydrate ($CuSO_4(H_2O)_5$) and human blood (1:100 dilution); were used to fill embedded vessels before PA imaging (Fig. 1. c).

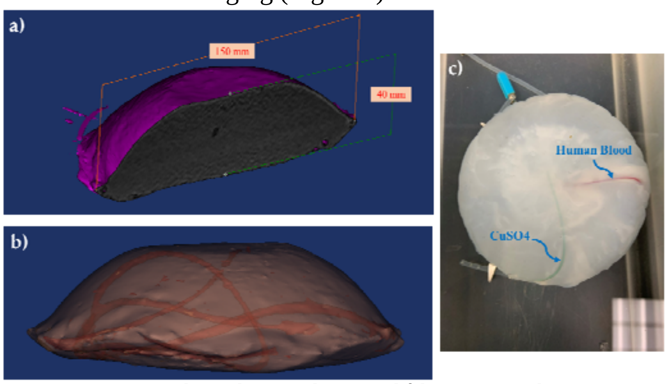

Fig. 1. Brain-mimicking phantom design and fabrication a) The dimensions of the phantom were about 150 × 40 mm, b) 3D model of the phantom including two simulated vessels with 1.2 and 1.4 mm inside diameters were inserted randomly to the phantom, c) The cross-section of the phantom with vessels are filled using two different contrast agents CuSO4(H2O)5 and human blood.

To acquire MR images of the phantom before any deformations, the phantom was scanned using a Siemens scanner 1.5 Tesla using a standard T_1 and T_2 weighted protocol. Pulse-sequence parameters were set to: T_R=600 ms, T_E=10 ms, Ec=1/1 27.8 KHz for T_1 weighted and T_R=8.6, T_E=3.2, T_I=450, Ec=1/1 31.3 KHz for T_2 weighted considering 1mm slice thickness with full brain phantom coverage and 1 mm isotropic resolution.

PA images were achieved by using ultrasound scanner (Vantage 128, Verasonics Inc., Kirkland, WA, USA) with a 128 elements linear array US transducer (L11-4v, Verasonics, Inc., Kirkland, WA, USA) operating at frequency range between 4 to 9 MHz. A pulsed tunable laser (PhocusCore, Optotek, California, USA) and Nd:YAG/OPO nanosecond pulsed laser (Phocus core system, OPOTEK Inc., USA), with the pulse repetition rate of 10 Hz at wavelengths of 700, 800, and 900 nm were used to illuminate the phantom. Scan resolution was 1 mm, and laser fluence was ~1 mJ/cm^2 (Fig. 2).

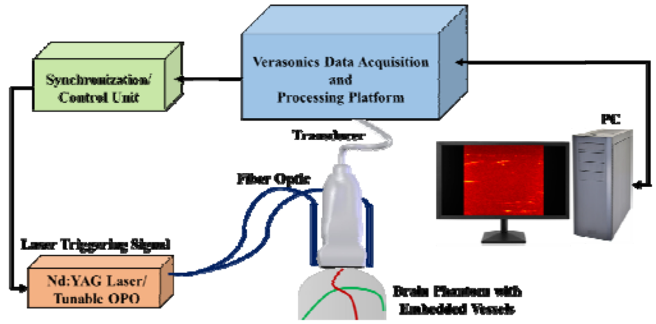

Fig. 2. Schematic of PA imaging setup which is including a tunable pulsed laser and a programmable ultrasound data acquisition system.

B. *Murine brain data*

For further evaluation of the proposed image registration method, we used ex-vivo mouse brain data which was provided by Ren. et al. in a previous study [67]. After removal of the mouse brain skull; the whole brain of mouse was embedded in agar 3% in phosphate-buffered saline and then was imaged ex-vivo. To acquire T_2-weighted MR images of mouse brain a 2-D spin echo sequence with imaging parameters of TR=2627.7 ms, TE=36 ms, slice thickness 0.7 mm, field of view 20 ×20 mm, and scanning time 12.36 min were used. For PA imaging the laser excitation pulses of 9 ns were delivered at five wavelengths (680, 715, 730, 760, 800, and 850 nm) in coronal orientation with field of view 20 mm ×20 mm, step sizes of 0.3 mm moving along horizontal direction, and scan time 20 of minutes. To validate these data, five natural anatomical landmarks were manually selected as registration targets (Fig. 3).

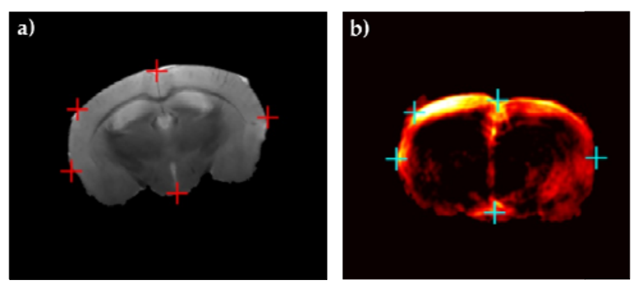

Fig. 3. Ex-vivo head of mouse data (a) MR image, (b) PA image, five registration targets is shown in red and blue point in a) and b) respectively, to assess the performance of registration algorithm [67].

C. *Inducing Brain Deformation*

The proposed algorithm was designed to compensate brain deformation during neurosurgery. Since the brain deformation is a complicated non-linear transformation, it is a challenging task to implement it physically on the phantom or mouse brain data. To evaluate our proposed registration algorithm, we performed brain deformation numerically by applying pre-defined pixel shifts to images. For this purpose, we used pre-operative and intra-operative MR images of brain tissue. The intra-operative MR image was considered as a gold standard. The deformation matrix was obtained by mono-modal registration of these images using residual complexity algorithm [70] (Fig. 4). Then the obtained brain deformation matrix was applied on PA images of brain phantom and mouse brain data.

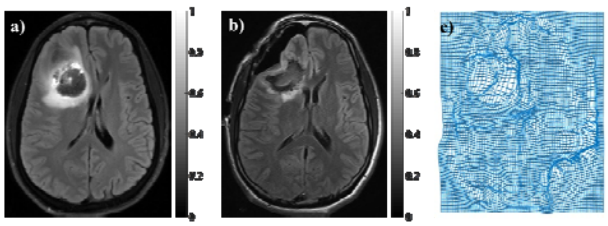

Fig. 4. (a) Pre-operative MR image, (b) Inta-operative MR image, (c) Brain deformation filed was achived by registration of intra-operative and pre-operative MR images using residual complexity method.

D. PA-MR Image Registration Framework

In the following, the workflow for automatic multi-modal image registration to compensate the brain deformation was shown in Fig. 5. After preparing two data set including brain-mimicking phantom data and murine brain data, pre-deformation MR images were setting as a reference images and pre-deformation PA image were setting as float images. Then a real brain deformation matrix which was achived by registration of intra-operative and pre-operative patient MR images using residual complexity method was applied on PA images to generate deformed PA images. Then by using proposed registration method based on joint co-sparse analysis, registration of MR image and deformed PA image was done. Finally, image registration results were evaluated and visualized for brain shift calculation. To evaluate the registration algorithm, root mean square error (RMSE) was calculated for phantom and mouse images registration. Additionally, target registration error (TRE) was calculated for defined targets in phantom and mouse brain data. Furthermore, we used the Hausdorff Distance (HD) between the PA and MR images. The HD between two point sets is defined as:

$$HD(I_{PA}, I_{MR}) = Max[Max\,Min\,d(I_{PA}, I_{MR}),\ Min\,Max\,d(I_{PA}, I_{MR})]$$

where, is the Euclidean distance of the locations, and smaller value of HD indicates a better alignment of boundaries. To avoid the effect of outliers [73], we used 95% HD instead of maximum HD.

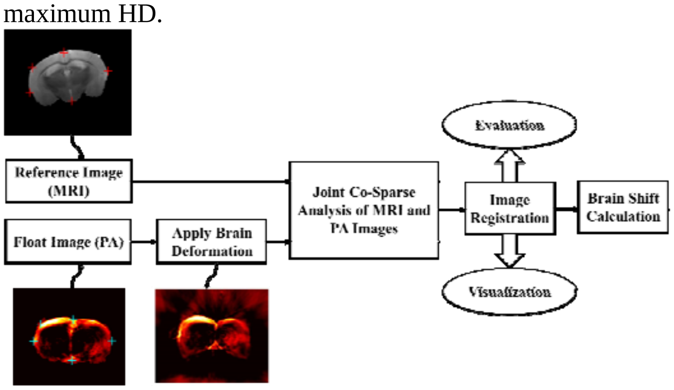

Fig. 5. The workflow for automatic multi-modal image registration to compensate brain deformation. MR and PA images including pre-defined targets were setting as reference and float images, respectively. After applying brain deformation on PA images, registration of MR and deformed PA was done and evaluated.

E. Co-sparse analysis model

Image (I) can be approximated via the sparse representation $x \in R^n$ which is a linear combination of a few non-zero elements (named atoms) in an over-complete dictionary matrix $D \in R^{n \times k}$ ($n << k$).

$$x \approx D\alpha \quad (1)$$

where $\alpha \in R^k$ is a sparse vector with the fewest k non-zero elements. The sparse coefficients describe the salient features of the images. Therefore, the sparse representation problem could be solved as the following optimization problem:

$$\min_{\alpha} \|\alpha\|_0, s.t \|x - D\alpha\|_2 \leq \varepsilon \quad (2)$$

Here, $\|\alpha\|_0$ is the zero norm of α that represents the number of non-zero values in a vector (α). The sparse representation of an image considers that a synthesis dictionary represents the redundant signals.

There is also another representation of image based on the co-sparse analysis model [60]. This alternative assumes that for a signal of interest (x), there exists an analysis operator $\Omega \in R^{k \times n}$ such that $\Omega x \approx \alpha$ as an analyzed vector is sparse for all $x \in R^n$. The rows of Ω represent filters that provide sparse responses and indices of the filters with zero response determine the subspace to which the signal belongs to. This subspace is the intersection of all hyperplanes to which these filters are normal vectors, and therefore, the information of signals is encoded in its zero responses. The index set of the zero entries of Ωx is called the *co-support* of x as below:

$$\mathrm{cosupp}(\Omega x) := \{ j \mid (\Omega x)_j = 0 \} \quad (3)$$

As the key property of analysis sparse models, these models put an emphasis on the zeros in the analysis representation rather than the non-zeros in the sparse representation of the signal. These zeros in the analysis representation model inscribe the low-dimensional subspace which the signal belongs to. Consequently, analysis operator learning procedures finds the suitable operator Ω for signal X as below:

$$\Omega^* \in \arg\min \sum_i \|\Omega x_i\|_0 \quad (4)$$

where Ω^* is the optimized operator Ω. In order to relax the co-sparsity assumption, the log-square function as a proper approximation of zero norm is used for large values of ν as below:

$$g(\alpha) := \sum_k \log(1 + \nu \alpha_k^2) \quad (5)$$

where ν is the positive weight. Therefore, (4) could be converted to:

$$\Omega^* \in \arg\min \sum_i g(\Omega x_i) \quad (6)$$

One should consider that there has been three main constraints on the Ω^* to avoid trivial solutions as below [71]:

i. The rows of Ω^* have unit Euclidean norm;

$$\Omega^* \in oblique \quad manifold \quad .$$

ii. The operator Ω^* has full rank, i.e., it has the maximal number of linear independent rows.

$$h(\Omega^*) = -\frac{1}{n\log(n)} \log\ \det(\frac{1}{m}\Omega^{*T}\Omega^*),$$

iii. The rows of the operator are not trivially linearly dependent.

$$r(\Omega^*) = -\sum_{k<1} \log(1-(\Omega_k{}^T\Omega_l)^2) \quad (7)$$

F. Multi-modal Image Registration Algorithm

In this study, we formulated the multimodal image registration problem in terms of an analysis co-sparse model. There are different co-sparse models that could be used in multimodal image registration approaches [72]. In our approach a joint analysis co-sparse model (JACSM) was proposed for registration of PA and MR images. JACSM indicates that different signals from different sensors of the same scene form an ensemble. The signals in an ensemble including a common sparse component; shared between all of them, and an innovation component which represents individual differences [73].

Consider two images I_{PA} and I_{MR} which are provided through PA and MR imaging, respectively, from brain simulated phantom as the input data. The interdependency of the two image modalities was modeled via JACSM and common sparse components were considered in this study. This images pair has a co-sparse representation with an appropriate pair of analysis operators $(\Omega_{PA}, \Omega_{MR}) \in R^{k\times n_{PA}} \times R^{k\times n_{MR}}$. By considering structures of images encoded in their co-supports based in equation (3), there is a pair of analysis operators so that the intersection of the co-supports of $\Omega_{PA} I_{PA}$ and $\Omega_{MR} I_{MR}$ is large. In specific, we try to learn the pair of co-sparse analysis operator $(\Omega_{PA}, \Omega_{MR})$ for two different image modalities.

On the other hand, the PA and MR images should be matched with a transformation T such that:

$$I_{MR}(Tx) \approx I_{PA}(x), \qquad for\ all\ pixel\ cordinate\ x \quad (8)$$

which x determines homogeneous pixel coordinates in PA images. The goal of multi-modal image registration problem in this approach is to optimize T by using the pair of analysis operators $(\Omega_{PA}, \Omega_{MR})$. We consider that for an optimized transformation, there is a coupled sparsity measure to be minimized. Thus, by considering equation (6) and constraints based on (7) we are searching for T^* such that:

$$T^* \in \arg\min \frac{1}{N}\sum_{i=1}^{N} g(\Omega_{PA} I_{PA}{}^{(i)}, \Omega_{MR} I_{MR}(Tx)^{(i)}) -$$
$$k \quad \frac{1}{n\log(n)}[\log\ \det(\frac{1}{m}\Omega_{MR}{}^{*T}\Omega_{MR}{}^{*}) + \log\ \det(\frac{1}{m}\Omega_{PA}{}^{*T}\Omega_{PA}{}^{*})] -$$
$$\mu \sum_{r<1} \log(1-(\Omega_{PA_r}{}^T\Omega_{PAl})^2) + \log(1-(\Omega_{MR_r}{}^T\Omega_{MRl})^2). \quad (9)$$

To tackle the problem of (9), we propose the ADMM. In other words, the analysis operators were learned by optimizing a JACSM via an ADMM. The ADMM as a candidate solver for convex problems, breaking our main problem into smaller sub-problems as below:

$$\min\ f(x) + g(y), \quad s.t.\ Ax + By = c \quad (10)$$

where $x \in R^n$, $y \in R^m$, $A \in R^{p\times n}$, and $B \in R^{p\times m}$. The augmentation Lagrangian for the equation (10) can be written as:

$$L_p(x,y,\lambda) = f(x) + g(y) + \lambda^T(Ax+By-c) + (\frac{\rho}{2})\|Ax+By-c\|_2^2 \quad (11)$$

where term ρ is a penalty term that is considered positive, and λ is the Lagrangian multiplier. Equation (11) is solved over three steps: x-minimization, and y-minimization, these two are split into N separate problems and followed by an updating step for multiplier λ as follows:

$$x^{k+1} := \arg\min_x L_p(x, y^k, \lambda^k),$$
$$y^{k+1} := \arg\min_y L_p(x^{k+1}, y, \lambda^k), \quad (12)$$
$$\lambda^{k+1} := \lambda^k + \rho(Ax^{k+1} + By^{k+1} - c).$$

III. Experiments & Results

To implement the proposed image registration algorithm, randomly, total of 20000 pairs of square sample patches of size 7 pixel from the total of images in the training set were selected. It is notable that in our experiments, the patch sizes 3, 5, 7, 9 and 11 pixels were applied. Based on our experience, small patch size would cause an over smooth effect, and a larger patch size would lead to more computation. Therefore, based on our results, the patch size of 7×7 was selected to balance the two effects.

The performance of JACSM based registration method was evaluated using a phantom with simulated vessels and using ex-vivo mouse brain data with anatomical landmarks. In Fig. 6, the performance of the proposed registration method for PA-MR, US-MR, and MR-MR images on the phantom data were shown and compared. In the first row, the MR image and its corresponding US and PA images were shown. Dashed yellow circles show the same fields of view in three different modalities (MRI, US, and PA). Corresponding structures which are used to calculate target registration error are labeled with numbers 1 to 3 in the three imaging modalities. The brain deformation field is applied to the images at the first row and the second row represents deformed MR, US, and PA images. As shown in Fig. 6. d, e, and f, labeled targets have been displaced due to inducing deformation. Finally, the images in the third row show the image registration results of MR, US, and PA after deformation (second row) with the original MRI before deformation (Fig. 6. a). The result of registration between the original MR image and deformed MR image (Fig. 6. g) is used as a gold standard to evaluate the proposed algorithm. Also, the registration result of deformed PA image (Fig. 6. i) is compared to registration result of deformed ultrasound image (Fig. 6. h) as a commonly used intra-operative imaging modality for brain shift compensation. As we have shown in the third row, images registered more accurate in MR-MR images registration compared to PA-MR image registration. Also, images registered more accurately in PA-MR image registration compared to the US-MR image registration. As we have shown with the blue arrow in the third-row images, the surface of the phantom is matched accurately in the result of MR-MR image registration. It is while, registration of US-MR has the worst performance to match the surface of the phantom in two modalities and registration of PA-MR has an acceptable performance to match the surface of phantom in two modalities PA and MRI.

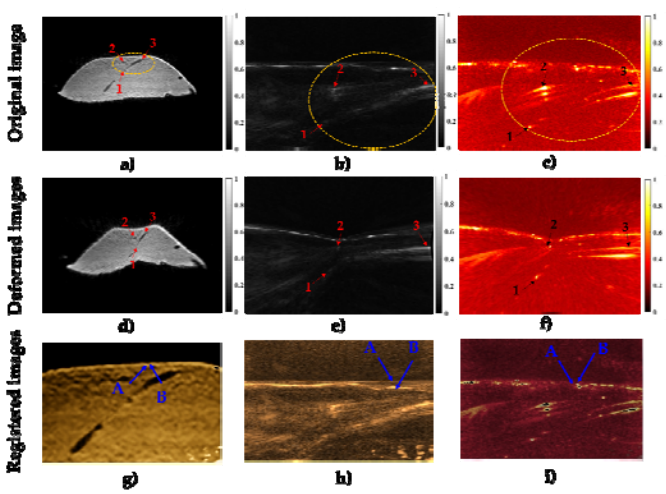

Fig 6. The results of multi-modal image registration of phantom data. First row: Original image of phantom data before deformation from three different modalities a) MRI, b) US, and c) PA, Second row: Deformed images of d) MRI, e) US,and f) PA. Third row show the results of registered images of g) MR-MR, f) US-MR, and g) PA-MR. Blue arrow in third row images represent the surface of phantom in different modalities. Blue arrow A are related to the surface of phantom in original MR images and blue arrows B are related to the surface of phantom in deformed MR, deformed US, and deformed PA images, in (g), (h) and (i), respectively.

To quantitative evaluation of the proposed registration method, RMSE, TRE, and HD for PA-MR, US-MR, and MR-MR image registration were calculated and shown in Table.1. Also, for further evaluation the results of our proposed method were compared to the commonly used normalized mutual information (NMI) registration method. In total, we used 23 phantom data. Registration accuracy of MR and MR images was considered as a gold standard. Also, the algorithms are

TABLE I
EVALUATION OF PROPOSED REGISTRATION METHODS ON PHANTOM DATA.

Multimodal Registration		RMSE (mean±std)	TRE (mean±std) Number of targets: 3	HD (mean±std)
MR-MR	JACSM	0.62±0.04	0.32±0.03	0.21±0.03
	NMI	0.98±0.09	0.51±0.04	0.46±0.07
US-MR	JACSM	1.17±0.13	0.96±0.08	0.51±0.03
	NMI	1.87±0.15	1.58±0.11	1.23±0.13
PA-MR	JACSM	0.73±0.05	0.58±0.04	0.32±0.04
	NMI	1.18±0.09	0.96±0.08	0.68±0.05

implemented in MATLAB, and tested on an Intel Corei7 3.2 GHz CPU with 8GB RAM.

The results of phantom study showed that PA-MR image registration has better RMSE, TRE and HD about 60%, 65% and 59% compared to US-MR image registration as a common imaging modality for brain shift compensation, respectively. On the other hand, the proposed method reached RMSE of about 0.73 mm which is acceptable in comparison with MR-MR image registration as a gold with RMSE of about 0.62 mm. The proposed method improved the results of RMSE and TRE of about 60% and 63% (on average) compared to NMI.

For further evaluation of the proposed method, the *ex-vivo* mouse brain data was used. In Fig. 7, the performance of JACSM based registration method for PA-MR image registration for mouse brain data were shown and compared with MR-MR image registration. Fig. 7. a and b represent MR and PA images of mouse brain before any deformation, respectively. The PA image after applying non-linear deformation is shown in Fig. 7. c, and the registration result of deformed PA and original MR of mouse brain images is shown in Fig. 7. d. Also, in panel (e) the mean of RMSE, TRE, and HD of PA-MR image registration for all data of mouse brain was calculated and compared to the result of MR-MR image registration.

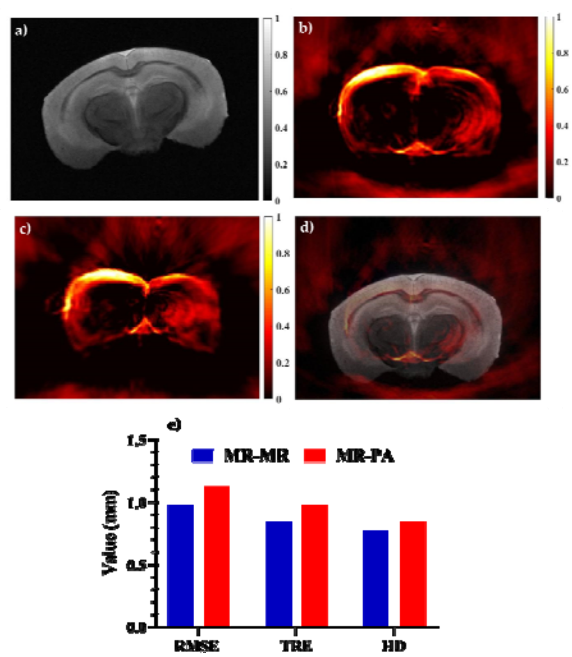

Fig. 7. The results of multi-modal image registration of mouse brain data. a) MRI, b) PA image, c) PA image after applying non-linear deformation, and d) registration of deformed PA and MRI of mouse data. Panel (e) shows the mean of RMSE, TRE, and HD of PA-MR image registration for all data of mouse brain.

The results acquired from *ex-vivo* mouse brain also proved the ability of the proposed registration method to recover non-linear deformation with calculated mean of RMSE, TRE, and HD as 1.13, 0.98, and 0.85 mm, respectively. The results are acceptable when compared to results of MRI-MRI registration as a gold standard with RMSE, TRE, and HD about 0.98, 0.85, and 0.77 mm. In fact, intra-operative PA as a real time imaging with about 15% RMSE increase, could be a good alternative for intra-operative MR imaging. Additionally, with 60% improvement in registration accuracy, PA imaging could be an alternative for intra-operative ultrasound imaging.

Having a closer look at the comparison between synthesis and analysis models, the synthesis model contains very few low-dimensional subspaces, and an increasingly large number of subspaces of higher dimension. In contrast, the analysis model includes a combinatorial number of low-dimensional subspaces with fewer high-dimensional subspaces. The co-sparse analysis models can yield richer feature representations, and joint co-sparse analysis models consider common sparse component of different signals from different sensors. Therefore, the JACSM based registration method to be more suitable for multi-modal images registration.

IV. Conclusion

There has been a growing interest in intra-operative imaging approaches to update the pre-operative images with real-time data when tissue deformation occurs during surgery. In specific, accurate and real-time brain shift compensation remains as a challenging problem during neurosurgery. In this study for the first time, we proposed application of PA imaging as interventional solution during neurosurgery in combination with pre-operative modalities, such as MRI to track brain deformation. However, accurate combination of PA and MR images requires the development of a real-time and robust image registration algorithm. Accurate registration of intra-operative PA images with pre-operative MR images of brain tissue could calculate and compensate brain deformation. In this study, the JACSM based registration is proposed for PA-MR image registration which can capture the interdependency of two modalities. The proposed algorithm works based on the minimization of mapping transform by using a pair of analysis operators in PA and MR images which are learned by the ADMM. The algorithm was tested on two data sets of phantom and mouse brain data and the results showed more accurate performance for PA imaging versus US imaging for brain shift calculation. Furthermore, the proposed method showed about 60% improvement in TRE in comparison with the common NMI registration method. The co-sparse analysis models can yield richer feature representations and better accuracy for medical image registration in the real time process which is crucial for surgeons during neurosurgery to compensate brain shift. Finally, by using this JACSM-based registration, the intra-operative PA images could become a promising tool when the brain shift invalidated pre-operative MRI.

Acknowledgment

The authors gratefully acknowledge the Dr. Ruiqing Ni from University of Zurich and ETH Zurich for providing mouse brain data.

References

[1] D. A. Orringer, A. Golby, and F. J. E. r. o. m. d. Jolesz, “Neuronavigation in the surgical management of brain tumors: current and future trends,” vol. 9, no. 5, pp. 491-500, 2012.

[2] I. J. Gerard, M. Kersten-Oertel, K. Petrecca, D. Sirhan, J. A. Hall, and D. L. Collins, “Brain shift in neuronavigation of brain tumors: A review,” *Medical image analysis,* vol. 35, pp. 403-420, 2017.

[3] Y. Xiao, H. Rivaz, M. Chabanas, M. Fortin, I. Machado, Y. Ou, M. P. Heinrich, J. A. Schnabel, X. Zhong, and A. Maier, “Evaluation of MRI to ultrasound registration methods for brain shift correction: The CuRIOUS2018 Challenge,” *IEEE Transactions on Medical Imaging,* 2019.

[4] I. J. Gerard, M. Kersten-Oertel, J. A. Hall, D. Sirhan, and D. L. J. F. i. O. Collins, “Brain Shift in Neuronavigation of Brain Tumors: An Updated Review of Intra-Operative Ultrasound Applications,” vol. 10, pp. 3390, 2021.

[5] T. Mitsui, M. Fujii, M. Tsuzaka, Y. Hayashi, Y. Asahina, and T. Wakabayashi, “Skin shift and its effect on navigation accuracy in image-guided neurosurgery,” *Radiological physics and technology,* vol. 4, no. 1, pp. 37-42, 2011.

[6] D. L. Hill, C. R. Maurer, R. J. Maciunas, R. J. Maciunas, J. A. Barwise, J. M. Fitzpatrick, and M. Y. Wang, “Measurement of intraoperative brain surface deformation under a craniotomy,” *Neurosurgery,* vol. 43, no. 3, pp. 514-526, 1998.

[7] M. A. Hammoud, B. L. Ligon, R. Elsouki, W. M. Shi, D. F. Schomer, and R. Sawaya, “Use of intraoperative ultrasound for localizing tumors and determining the extent of resection: a comparative study with magnetic resonance imaging,” *Journal of neurosurgery,* vol. 84, no. 5, pp. 737-741, 1996.

[8] O. Škrinjar, A. Nabavi, and J. J. M. i. a. Duncan, “Model-driven brain shift compensation,” vol. 6, no. 4, pp. 361-373, 2002.

[9] A. Wittek, R. Kikinis, S. K. Warfield, and K. Miller, "Brain shift computation using a fully nonlinear biomechanical model." pp. 583-590.

[10] M. I. Miga, K. Sun, I. Chen, L. W. Clements, T. S. Pheiffer, A. L. Simpson, R. C. J. I. j. o. c. a. r. Thompson, and surgery, “Clinical evaluation of a model-updated image-guidance approach to brain shift compensation: experience in 16 cases,” vol. 11, no. 8, pp. 1467-1474, 2016.

[11] P. Grunert, W. Müller-Forell, K. Darabi, R. Reisch, C. Busert, N. Hopf, and A. J. C. A. S. Perneczky, “Basic principles and clinical applications of neuronavigation and intraoperative computed tomography,” vol. 3, no. 4, pp. 166-173, 1998.

[12] C. Nimsky, O. Ganslandt, S. Cerny, P. Hastreiter, G. Greiner, and R. J. N. Fahlbusch, “Quantification of, visualization of, and compensation for brain shift using intraoperative magnetic resonance imaging,” vol. 47, no. 5, pp. 1070-1080, 2000.

[13] D. Kuhnt, M. H. Bauer, and C. J. C. R. i. B. E. Nimsky, “Brain shift compensation and neurosurgical image fusion using intraoperative MRI: current status and future challenges,” vol. 40, no. 3, 2012.

[14] O. Clatz, H. Delingette, I.-F. Talos, A. J. Golby, R. Kikinis, F. A. Jolesz, N. Ayache, and S. K. Warfield, “Robust nonrigid registration to capture brain shift from intraoperative MRI,” *IEEE transactions on medical imaging,* vol. 24, no. 11, pp. 1417-1427, 2005.

[15] P. A. Valdés, X. Fan, S. Ji, B. T. Harris, K. D. Paulsen, D. W. J. S. Roberts, and f. neurosurgery, “Estimation of brain deformation for volumetric image updating in protoporphyrin IX fluorescence-guided resection,” vol. 88, no. 1, pp. 1-10, 2010.

[16] J. W. Trobaugh, W. D. Richard, K. R. Smith, and R. D. Bucholz, “Frameless stereotactic ultrasonography: method and

applications," *Computerized Medical Imaging and Graphics,* vol. 18, no. 4, pp. 235-246, 1994.
[17] A. Roche, X. Pennec, M. Rudolph, D. Auer, G. Malandain, S. Ourselin, L. M. Auer, and N. Ayache, "Generalized correlation ratio for rigid registration of 3D ultrasound with MR images." pp. 567-577.
[18] J. Koivukangas, J. Ylitalo, E. Alasaarela, and A. Tauriainen, "Three-dimensional ultrasound imaging of brain for neurosurgery," *Annals of clinical research,* vol. 18, pp. 65-72, 1986.
[19] P. Farnia, A. Ahmadian, T. Shabanian, N. D. Serej, and J. Alirezaie, "Brain-shift compensation by non-rigid registration of intra-operative ultrasound images with preoperative MR images based on residual complexity," *International journal of computer assisted radiology and surgery,* vol. 10, no. 5, pp. 555-562, 2015.
[20] S. Bayer, A. Maier, M. Ostermeier, and R. J. I. j. o. b. i. Fahrig, "Intraoperative imaging modalities and compensation for brain shift in tumor resection surgery," vol. 2017, 2017.
[21] P. Farnia, M. Mohammadi, E. Najafzadeh, M. Alimohamadi, B. Makkiabadi, and A. Ahmadian, "High-quality photoacoustic image reconstruction based on deep convolutional neural network: towards intra-operative photoacoustic imaging," *Biomedical Physics & Engineering Express*, 2020.
[22] M. Pramanik, G. Ku, C. Li, and L. V. Wang, "Design and evaluation of a novel breast cancer detection system combining both thermoacoustic (TA) and photoacoustic (PA) tomography," *Medical physics,* vol. 35, no. 6Part1, pp. 2218-2223, 2008.
[23] M. Mehrmohammadi, S. Joon Yoon, D. Yeager, and S. J. C. M. I. Y Emelianov, "Photoacoustic imaging for cancer detection and staging," vol. 2, no. 1, pp. 89-105, 2013.
[24] E. Najafzadeh, H. Ghadiri, M. Alimohamadi, P. Farnia, M. Mehrmohammadi, and A. Ahmadian, "Application of multi-wavelength technique for photoacoustic imaging to delineate tumor margins during maximum-safe resection of glioma: A preliminary simulation study," *Journal of Clinical Neuroscience*, 2019.
[25] S. Arabpou, E. Najafzadeh, P. Farnia, A. Ahmadian, H. Ghadiri, and M. S. A. Akhoundi, "Detection of Early Stages Dental Caries Using Photoacoustic Signals: The Simulation Study," *Frontiers in Biomedical Technologies*, 2019.
[26] C. Moore, Y. Bai, A. Hariri, J. B. Sanchez, C.-Y. Lin, S. Koka, P. Sedghizadeh, C. Chen, and J. V. Jokerst, "Photoacoustic imaging for monitoring periodontal health: A first human study," *Photoacoustics,* vol. 12, pp. 67-74, 2018.
[27] Y. Yan, S. John, M. Ghalehnovi, L. Kabbani, N. A. Kennedy, and M. J. S. r. Mehrmohammadi, "photoacoustic Imaging for Image-guided endovenous Laser Ablation procedures," vol. 9, no. 1, pp. 1-10, 2019.
[28] E. Petrova, H. Brecht, M. Motamedi, A. Oraevsky, S. J. P. i. M. Ermilov, and Biology, "In vivo optoacoustic temperature imaging for image-guided cryotherapy of prostate cancer," vol. 63, no. 6, pp. 064002, 2018.
[29] B. Eddins, and M. A. L. J. J. o. b. o. Bell, "Design of a multifiber light delivery system for photoacoustic-guided surgery," vol. 22, no. 4, pp. 041011, 2017.
[30] L. V. Wang, and S. Hu, "Photoacoustic tomography: in vivo imaging from organelles to organs," *science,* vol. 335, no. 6075, pp. 1458-1462, 2012.
[31] L. V. Wang, and J. Yao, "A practical guide to photoacoustic tomography in the life sciences," *Nature methods,* vol. 13, no. 8, pp. 627, 2016.
[32] A. B. E. Attia, G. Balasundaram, M. Moothanchery, U. Dinish, R. Bi, V. Ntziachristos, and M. Olivo, "A review of clinical photoacoustic imaging: Current and future trends," *Photoacoustics*, pp. 100144, 2019.
[33] P. Beard, "Biomedical photoacoustic imaging," *Interface focus,* vol. 1, no. 4, pp. 602-631, 2011.
[34] A. Rosencwaig, and A. Gersho, "Theory of the photoacoustic effect with solids," *Journal of Applied Physics,* vol. 47, no. 1, pp. 64-69, 1976.
[35] S. Zackrisson, S. Van De Ven, and S. Gambhir, "Light in and sound out: emerging translational strategies for photoacoustic imaging," *Cancer research,* vol. 74, no. 4, pp. 979-1004, 2014.
[36] M. Xu, and L. V. Wang, "Photoacoustic imaging in biomedicine," *Review of scientific instruments,* vol. 77, no. 4, pp. 041101, 2006.
[37] P. Farnia, E. Najafzadeh, A. Hariri, S. N. Lavasani, B. Makkiabadi, A. Ahmadian, and J. V. Jokerst, "Dictionary learning technique enhances signal in LED-based photoacoustic imaging," *Biomedical Optics Express,* vol. 11, no. 5, pp. 2533-2547, 2020.
[38] C. Hoelen, F. De Mul, R. Pongers, and A. Dekker, "Three-dimensional photoacoustic imaging of blood vessels in tissue," *Optics letters,* vol. 23, no. 8, pp. 648-650, 1998.
[39] P. Raumonen, and T. Tarvainen, "Segmentation of vessel structures from photoacoustic images with reliability assessment," *Biomedical optics express,* vol. 9, no. 7, pp. 2887-2904, 2018.
[40] E. Najafzadeh, H. Ghadiri, M. Alimohamadi, P. Farnia, M. Mehrmohammadi, and A. Ahmadian, "Evaluation of multi‐wavelengths LED‐based photoacoustic imaging for maximum safe resection of glioma: a proof of concept study," *International Journal of Computer Assisted Radiology and Surgery*, 2020.
[41] M. S. Karthikesh, X. J. E. B. Yang, and Medicine, "Photoacoustic image-guided interventions," vol. 245, no. 4, pp. 330-341, 2020.
[42] S. H. J. N. Han, "Review of photoacoustic imaging for imaging-guided spinal surgery," vol. 15, no. 4, pp. 306, 2018.
[43] K. P. Kubelick, S. Y. J. U. i. M. Emelianov, and Biology, "A Trimodal Ultrasound, Photoacoustic and Magnetic Resonance Imaging Approach for Longitudinal Post-operative Monitoring of Stem Cells in the Spinal Cord," vol. 46, no. 12, pp. 3468-3474, 2020.
[44] D. H. Iversen, W. Wein, F. Lindseth, G. Unsgård, and I. Reinertsen, "Automatic intraoperative correction of brain shift for accurate neuronavigation," *World neurosurgery,* vol. 120, pp. e1071-e1078, 2018.
[45] I. Reinertsen, M. Descoteaux, K. Siddiqi, and D. L. Collins, "Validation of vessel-based registration for correction of brain shift," *Medical image analysis,* vol. 11, no. 4, pp. 374-388, 2007.
[46] S. J.-S. Chen, I. Reinertsen, P. Coupé, C. X. Yan, L. Mercier, D. R. Del Maestro, and D. L. Collins, "Validation of a hybrid Doppler ultrasound vessel-based registration algorithm for neurosurgery," *International journal of computer assisted radiology and surgery,* vol. 7, no. 5, pp. 667-685, 2012.
[47] P. Farnia, A. Ahmadian, A. Khoshnevisan, A. Jaberzadeh, N. D. Serej, and A. F. Kazerooni, "An efficient point based registration of intra-operative ultrasound images with MR images for computation of brain shift; A phantom study." pp. 8074-8077.
[48] T. Arbel, X. Morandi, R. M. Comeau, and D. L. Collins, "Automatic non-linear MRI-ultrasound registration for the correction of intra-operative brain deformations." pp. 913-922.
[49] S. Ji, A. Hartov, D. Roberts, and K. Paulsen, "Mutual-information-corrected tumor displacement using intraoperative ultrasound for brain shift compensation in image-guided neurosurgery." p. 69182H.
[50] W. Wein, A. Ladikos, B. Fuerst, A. Shah, K. Sharma, and N. Navab, "Global registration of ultrasound to MRI using the LC 2 metric for enabling neurosurgical guidance." pp. 34-41.
[51] P. Coupé, P. Hellier, X. Morandi, and C. Barillot, "3D rigid registration of intraoperative ultrasound and preoperative MR brain images based on hyperechogenic structures," *Journal of Biomedical Imaging*, vol. 2012, pp. 1, 2012.
[52] H. Rivaz, Z. Karimaghaloo, and D. L. Collins, "Self-similarity weighted mutual information: a new nonrigid image registration metric," *Medical image analysis,* vol. 18, no. 2, pp. 343-358, 2014.
[53] H. Rivaz, S. J.-S. Chen, and D. L. Collins, "Automatic deformable MR-ultrasound registration for image-guided neurosurgery," *IEEE transactions on medical imaging,* vol. 34, no. 2, pp. 366-380, 2015.
[54] I. Machado, M. Toews, E. George, P. Unadkat, W. Essayed, J. Luo, P. Teodoro, H. Carvalho, J. Martins, and P. Golland, "Deformable MRI-ultrasound registration using correlation-based attribute matching for brain shift correction: Accuracy and generality in multi-site data," *NeuroImage,* vol. 202, pp. 116094, 2019.
[55] Q. Zhang, Y. Liu, R. S. Blum, J. Han, and D. Tao, "Sparse representation based multi-sensor image fusion for multi-focus and multi-modality images: A review," *Information Fusion,* vol. 40, pp. 57-75, 2018.
[56] P. Farnia, A. Ahmadian, T. Shabanian, N. D. Serej, and J. Alirezaie, "A hybrid method for non-rigid registration of intra-operative ultrasound images with pre-operative MR images." pp. 5562-5565.

[57] P. Farnia, B. Makkiabadi, A. Ahmadian, and J. Alirezaie, "Curvelet based residual complexity objective function for non-rigid registration of pre-operative MRI with intra-operative ultrasound images." pp. 1167-1170.

[58] K. Huang, and S. Aviyente, "Sparse representation for signal classification." pp. 609-616.

[59] A. Roozgard, N. Barzigar, P. Verma, and S. Cheng, “3D-SCoBeP: 3D medical image registration using sparse coding and belief propagation,” *International Journal of Diagnostic Imaging,* vol. 2, no. 1, pp. 54, 2014.

[60] S. Nam, M. E. Davies, M. Elad, and R. Gribonval, “The cosparse analysis model and algorithms,” *Applied and Computational Harmonic Analysis,* vol. 34, no. 1, pp. 30-56, 2013.

[61] N. Zhou, H. Jiang, L. Gong, and X. Xie, “Double-image compression and encryption algorithm based on co-sparse representation and random pixel exchanging,” *Optics and Lasers in Engineering,* vol. 110, pp. 72-79, 2018.

[62] M. Kiechle, S. Hawe, and M. Kleinsteuber, "A joint intensity and depth co-sparse analysis model for depth map super-resolution." pp. 1545-1552.

[63] M. Kiechle, T. Habigt, S. Hawe, and M. Kleinsteuber, “A bimodal co-sparse analysis model for image processing,” *International Journal of Computer Vision,* vol. 114, no. 2-3, pp. 233-247, 2015.

[64] C. Han, H. Zhang, C. Gao, C. Jiang, N. Sang, and L. Zhang, “A Remote Sensing Image Fusion Method Based on the Analysis Sparse Model,” *IEEE Journal of Selected Topics in Applied Earth Observations and Remote Sensing,* vol. 9, no. 1, pp. 439-453, 2016.

[65] R. Gao, S. A. Vorobyov, and H. Zhao, “Image fusion with cosparse analysis operator,” *IEEE Signal Processing Letters,* vol. 24, no. 7, pp. 943-947, 2017.

[66] P. Farnia, E. Najafzadeh, A. Ahmadian, B. Makkiabadi, M. Alimohamadi, and J. Alirezaie, "Co-sparse analysis model based image registration to compensate brain shift by using intra-operative ultrasound imaging." pp. 1-4.

[67] W. Ren, H. Skulason, F. Schlegel, M. Rudin, J. Klohs, and R. Ni, “Automated registration of magnetic resonance imaging and optoacoustic tomography data for experimental studies,” *Neurophotonics,* vol. 6, no. 2, pp. 025001, 2019.

[68] M. Gehrung, M. Tomaszewski, D. McIntyre, J. Disselhorst, and S. Bohndiek, “Co-Registration of Optoacoustic Tomography and Magnetic Resonance Imaging Data from Murine Tumour Models,” *Photoacoustics,* pp. 100147, 2020.

[69] K. Surry, H. Austin, A. Fenster, and T. Peters, “Poly (vinyl alcohol) cryogel phantoms for use in ultrasound and MR imaging,” *Physics in Medicine & Biology,* vol. 49, no. 24, pp. 5529, 2004.

[70] A. Myronenko, and X. Song, “Intensity-based image registration by minimizing residual complexity,” *IEEE transactions on medical imaging,* vol. 29, no. 11, pp. 1882-1891, 2010.

[71] S. Hawe, M. Kleinsteuber, and K. Diepold, “Analysis operator learning and its application to image reconstruction,” *IEEE Transactions on Image Processing,* vol. 22, no. 6, pp. 2138-2150, 2013.

[72] S. Cai, Z. Kang, M. Yang, X. Xiong, C. Peng, and M. J. S. Xiao, “Image denoising via improved dictionary learning with global structure and local similarity preservations,” vol. 10, no. 5, pp. 167, 2018.

[73] Q. Zhang, Y. Fu, H. Li, and J. Zou, “Dictionary learning method for joint sparse representation-based image fusion,” *Optical Engineering,* vol. 52, no. 5, pp. 057006, 2013.